Mechanical and morphological characterization of capacitor discharge welding of an automotive material AA6061

Thesis for master degree of Automotive Engineering

Candidate: Tang Yingxiao
Tutor: Giovanni Maizza
2018/2/22

Index

Figure list

Table list

Abstract

The aluminum alloys are more and more exploited as a light-weight material in the transportation industry in order to improve the fuel efficiency and reduce the greenhouse gas emission. The 6061 aluminum alloy, which has properties of moderately high strength, good corrosion resistance, good weldability and formability is widely used for transportation and architecture applications.

Welding is one of the most important aspects of manufacturing operations whether it involves joining small electronic components or large structures, especially in the automotive industry. Capacitor discharge welding (CDW) is considered as an ideal option of welding in automotive industry with advantages of high efficiency which are in favour of high-volume and automatic production.

In this thesis, efforts were made to develop a methodology to characterize the welding joint of CDW of AA6061. Firstly, the metallographic analysis was implemented to understand the morphological change during welding. Then the Macroinstrumented indentation test was carried out to measure the mechanical properties of the welding joint. The MIIT is a valuable means to characterize the mechanical properties of the welding joints in a peculier region while permitting a correlation with conventional tensile test properties. The result shows a softening of the material that can be explained by the morphological changes.

This thesis might be useful for the automotive producers to establish a standard of welding and to the test of welding joints. Further research, such as the change of material properties under various welding parameters, is required as well.

【Keywords】: Aluminum alloys; AA6061; Capacitor discharge welding; Macroinstrumented indentation test.

Acknowledgement

I would first like to my thesis tutor Prof. Giovanni Maizza of the DISAT at Politecnico di Torino. The door to Prof. Giovanni office was always open whenever I had any question about my research or writing.

I would also like to thank Frediano De Marco and Renato Pero who helped me on the experiments. Without their contribution, the experiments could not have been successfully finished.

I would also like to acknowledge the laboratory members who gave me a hand during my project and who provided valuable output for me.

Finally, I must express my very profound gratitude to my parents for providing me with unfailing support and continuous encouragement throughout my years of study and through the process of researching and writing this thesis. This accomplishment would not have been possible without them. Thank you.

Tang Ying Xiao

Chapter 1 Introduction

1.1 Background

The blooming of the automotive industry and the continuous increasing of fossil fuel consumption is becoming the largest sources of anthropogenic greenhouse gas emission [1] [2]. Thus the strategies to improve fuel efficiency and reduce greenhouse gas emission are been continuously exploring by the transportation industry, the largest consumer of fossil fuel. These strategies include weight reduction, improving conventional engine efficiency, developing new and more energy efficient powertrains, such as electric and hybrid systems, and the use of low CO_2 fuels, such as biofuels [3][4].

Of these strategies, weight reduction has been identified as the most cost-effective. On the average, for a vehicle, the fuel consumption reduces by 0.5L per 100km [5], [6] and a reduction of 9 g of CO_2 per km [7].

Generally, for every 10 % weight reduction, the specific fuel consumption could reduce by 3–7 %, while maintaining the same functionality [1][2][3]. As a result, lightweight materials are increasingly being developed and incorporated into automotive and aerospace structures [4][8].

Owing to their low density, approximately one third that of steel, and high strength and stiffness to weight ratio, Al alloys have great potentials for weight reduction. In most applications, they allow a weight saving of up to 50 % over conventional materials without compromising strength and safety. Al alloys also possess excellent corrosion resistance, low-energy formability, good crashworthiness, high thermal and electrical conductivities, high reflectivity to both heat radiation and light, good machinability, and mass production capabilities at a reasonable price [7],[9]-[17]. Furthermore, they have excellent recyclability, and low secondary energy cost, which enables the Al industry to recycle all available scrap with only about 5 % of the energy required to produce new Al alloys. Thus, Al alloys attract tremendous attention in aerospace, naval, automotive, and other industries, in a variety of product forms— sheet, casting, and extrusion. Some applications of Al in vehicles include in body panels, power trains, closures, chassis, brake housings, air deflector parts, and seat slides [18]. In the future, they are expected to replace steel as the primary construction material in the automotive industry [7],[10][19]-[23]. For a North American light duty vehicle, for instance, there is a projected increase in net Al content from

394lb per vehicle in 2015 to about 547lb per vehicle in 2025 [24].

Welding is one of the most important aspects of manufacturing operations whether it involves joining small electronic components or large structures, especially in the automotive industry. It is also complex, since a number of metallurgical changes occur during the process [25]. There are approximately 5000 spot welds in a single automobile [27]-[30]. The quality, structural performance, lifespan, safety design, strength, stiffness, and integrity of a vehicle depend not only on the mechanical properties of the sheets but also on the quality of spot welds. Furthermore, the vehicle crashworthiness, which is defined as the capability of a car structure to provide adequate protection to its passengers against injuries in the event of a crash, largely depends on the integrity and the mechanical performance of spot welds [29], [31], [32].

Capacitor discharge welding (CDW) is a variation of stud welding. Although it has long been in existence, this process has not been extensively used primarily due to the lack of familiarity and understanding of the metallurgy and parameters of the process. Several researchers have investigated the process and developed models to represent the process physics. CDW has been found to be a rapid solidification process (RSP) with great benefits in terms of metallurgy and manufactory [26].

Some advantages of the process include a narrow heat affected zone, thin weld zones, on-line quality monitoring, short welding times, and high cooling rates permitting the joining of dissimilar metals. These features makes it ideal to automotive industry, high-volume and automatic production [25].

CDW has been used at a limited level because of the lack of available process knowledge. Therefore, the growing interest in high-volume CDW of Al alloys is accompanied with a challenge to better understand and improve the process, structure, properties, and performance relationships.

1.2 Research objective

The aim of this thesis is to characterize the microstructure and the mechanical property of the CDW by 6061 aluminum alloy, in order to establish a standard for the vehicle producer, providing a procedure of research.

Investigation of specific influence of CDW on the AA6061 is needed in order to have a better understanding of the effect of microstructure on the mechanical properties. The alloy was tested with optical microscopy observations, comparing the base material and the welding zone.

Instrumented indentation test was then carried out. The result of the macro instrumented indentation test of different points on the sample are compared with each other and with the typical values documented in the published literature in order to establish differences in the mechanical properties.

Chapter 2 Literature review

2.1 6XXX series of aluminum alloys

The 6xxx series Al alloys are widely used as medium strength structural alloys for transportation and architecture applications. The 6xxx series are versatile, heat treatable, highly formable, weldable and have moderately high strength coupled with excellent corrosion resistance [34].

Aluminum alloys contain impurities which affect grain structures and microstructures within the grains, meanwhile the other properties (Table 1). The presence of the impurities allows the alloys to respond differently to working and heat treating. The properties of 6xxx Al-Mg-Si alloys have been known to be influenced by the formation of precipitation Mg2Si (β) [35].

In this thesis, the experiments were made by 6061 aluminum alloy whose mechanical properties are shown in Table 2.

Composition (%)	6063	6005A	6061
Si	0.20-0.60	0.50-0.90	0.40-0.80
Fe	Max 0.35	0.00-0.35	Max 0.70
Cu	Max 0.10	0.00-0.30	0.15-0.40
Mn	Max 0.10	0.00-0.50	Max 0.15
Mg	0.45-0.90	0.40-0.70	0.80-1.20
Cr	Max 0.10	0.00-0.30	0.04-0.35
Zn	Max 0.10	0.00-0.20	Max 0.25
Ti	Max 0.10	0.00-0.10	Max 0.15
Max other (each)	Max 0.05	Max 0.05	Max 0.05
Max other (total)	Max 0.15	Max 0.15	Max 0.15

Table 1 Nominal chemical composition of three 6XXXs' series aluminum alloys

	Tensile strength		Yield strength		Elongation %		Shear strength	
Temper	MPa	ksi	Mpa	ksi	1.6mm thick specimen	13mm diam specimen	Mpa	ksi
O	124	18	55	8	25	30	83	12
T4, T451	241	35	145	21	22	25	165	24
T6, T651	310	45	276	40	12	17	207	30

Table 2 Typical mechanical properties of alloy 6061 used in the experiments

2.2 Capacitor discharge welding

In CDW, DC impulse of high intensity is discharged by a capacitor bank. Energy in the bank is absorbed from the network and stored during dead time. Figure 1 shows a typical time-current curve during capacitor discharge.

Capacitive resistance welders, also called capacitive discharge or CD welders, have many advantages over other welder types. Weld zone formation takes place during the first few milliseconds of the welding process. A CD welder allows extremely fast energy release with large peak currents. The larger the energy delivered in the weld region, the lower the energy dissipated as heat in the surrounding material. The heat affected zone, where the properties of the metal have been changed by rapid heating and cooling, is localized into a very small region around the weld. The high discharge rate of CD welders also allows electrically and thermally conductive materials, such as copper or aluminum, to be welded. Capacitor welders deliver repeatable welds even during line voltage fluctuations because weld energy is stored before use [33].

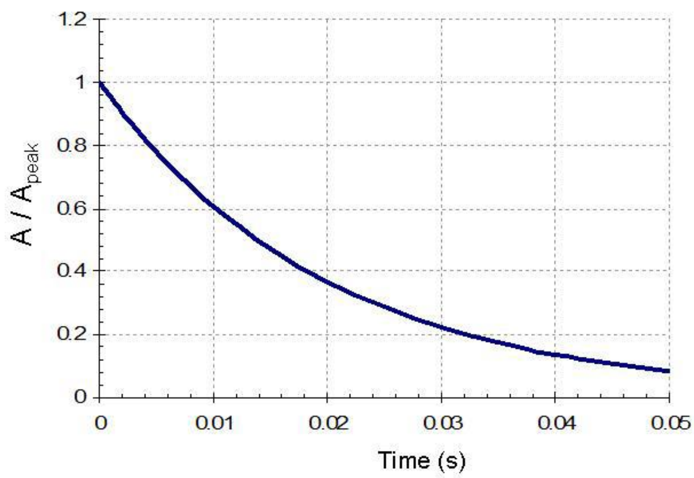

Figure 1 Sample capacitor discharge curve

Figure 2 shows several electrode configurations used in resistance welding. Figure 2a is called a direct weld. Current flows from upper electrode to the lower one, through the sheets to be welded. Figure 2b shows a step electrode configuration. This configuration is used when there is access to only one side of the workpiece and one electrode can be placed on both materials. Figure 2c is a series configuration. Electrodes can only be placed on one metal surface from one side. Current is divided between the two parts. This weld configuration requires more weld energy [33].

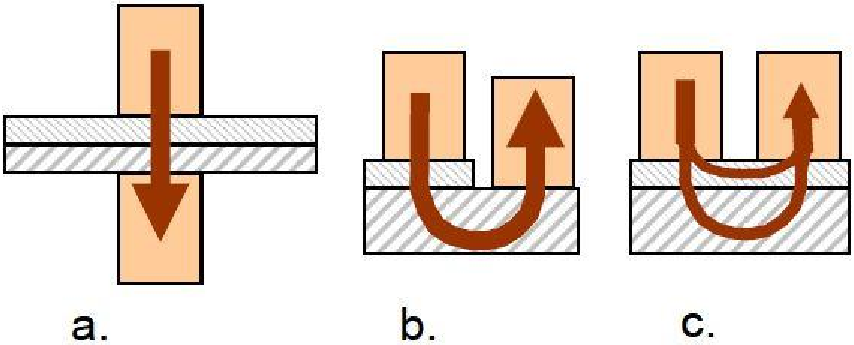

Figure 2 Examples of resistance welding electrode configurations: a.) direct, b.) step, c.) series.

The CDW process is typically featured by the following steps:

1) Place two or more overlapping metal sheets between two air-cooled or water-cooled (usually copper) electrodes.

2) Apply the load upon the electrodes so as to clamp the metal sheets together and also create sufficient contact between them.

3) Current discharge to the welding sheets via the two electrodes to the sheets for a specific period of time. Heat is generated by Joule dissipation of the sheets; as a result, a solid state nugget is formed at the faying interface.

4) Current switch-off and the electrode pressure is maintained and thus welding zone begins to cool rapidly. The fast cooling of the weld region is ensured by heat conduction through the two air-cooled electrodes and horizontally outwards through the sheets [36]-[39].

Classic Resistance Spot Welding (RSW) relies on metal resistivity (resistance) to heat and weld the alloys. A large current is passed through the metallic workpieces. Energy is dissipated due to the metal resistivity in the form of heat which heats up and welds the materials. There are two phases to the melting process. The welder must overcome both the material contact resistance and the bulk resistance of the two sheet materials. Figure 3 shows an example of a micro-scale surface profile. On the micro-scale, material surfaces are rough and contact occurs in a limited number of points. In the first few milliseconds of weld formation the high-resistance metal bridges recrystallize allowing other bridges to come into contact to continue the recrystallization process. When all of the bridges have been bonded the contact resistance is zero. The bulk resistance of the metal then plays the final role in the weld formation and rapid cooling.

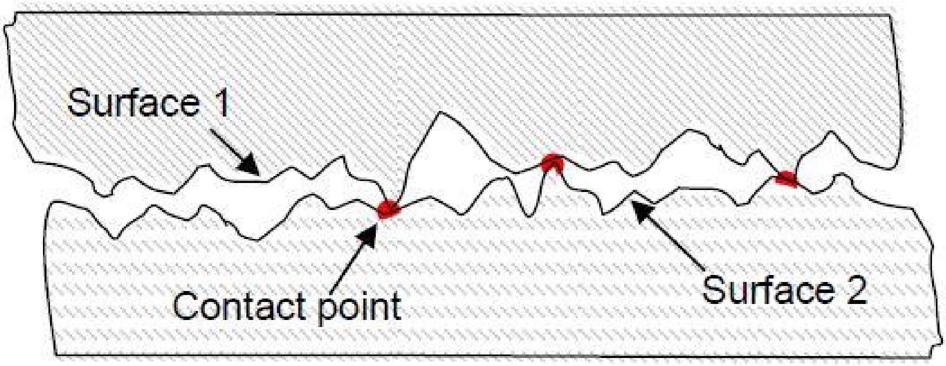

Figure 3 On the micro-scale surface roughness limits surface to surface contact. More contact points results in a lower contact resistance.

Several other factors play a part in the contact resistance. The larger the contact resistance is, the hotter the weld is. On the micro-scale, contact resistance is reduced when more metal bridges or contact points are formed (see Figure 3). Higher electrode pressure determines more uniform contact surface. This results in a lower contact resistance and cooler weld. Conversely, low electrode pressure results in lower contact area, higher resistance, and a hotter weld.

One way contact resistance can be controlled is through the pressure over the electrodes. High electrode pressure reduces contact resistance because the pressure creates more contact points (Figure 3). When contact resistance is reduced, less weld energy is consumed at the interface and therefore the weld is cooler. Conversely, lower weld pressure translates to higher contact resistance and a hotter weld. Electrode pressure also contributes to weld strength. The applied pressure forces the heated metal to mix together and to recrystallize. An appropriate amount of pressure should be used to ensure proper weld zone formation. Table 3 demonstrates how electrode pressure affects weld formation [33].

Pressure	**Weld heat**	**Weld strength**
Up	↓	↑
Down	↑	↓

Table 3 Weld properties with electrode pressure

2.3 Instrumented indentation test

Instrumented indentation test records the loads and the displacements of an indenter during a controlled loading-holding-unloading indentation cycle by means of specific sensors. The quantities measured at the same time are the applied force F and the indentation depth h. Force measurement is very accurate since the force transducers have typical uncertainties of less than0.5% of the applied force and a zero error nearly negligible, but indentation depth is strongly affected by the measurement device due to the frame compliance contribution. These acquisitions result in the so-called indentation curves (ICs), as depicted in Figure 4 [45].

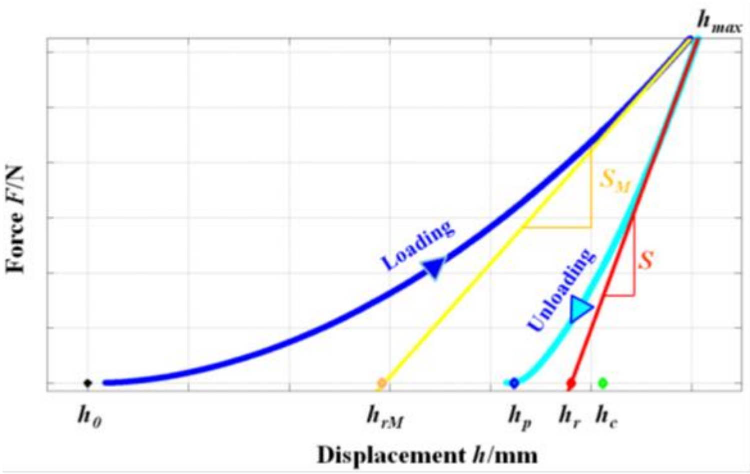

Figure 4 Schematic of an indentation curve.

- h_0: the zero point, i.e. the first point of contact

- h_{max}: the maximum depth of penetration of the tip into the sample

- F_{max}: the maximum applied load

- S_M: the tangent to the loading curve at h_{max}

- h_{rM}: the intercept of the tangent to the loading curve at h_{max}

- S: the tangent to the unloading curve at h_{max}

- h_r: the intercept of the tangent to the unloading curve at hmax

- h_c: the contact depth.

- h_p: the plastic depth, i.e. the last contact point corresponding to the result of the plastic deformation of the residual indentation when the elastic deformation is fully recovered.

Traditional Brinell and Vickers hardness are established after the complete withdrawal of the indenter by neglecting the elastic deformation in the diameter of the residual indentation. Thus, the corresponding sloping area A_s does not take into account the change in the depth of penetration due to the elastic recovery. Nevertheless, they are conventionally considered as test under loads. For metals, this is a widespread assumption even if it is experimentally proved that the small elastic recovery of the indentation leads to a contraction of the residual indentation diameter [46],[47]. Conversely, in IIT the contact area A_c is tightly related to the contact depth hc and hence to the fact that, after the withdraw of the indenter, the change in the indentation depth due to the elastic recovery may be not negligible. This assumption may pose some restriction on the direct comparison between the IIT results and the conventional Vickers counterpart.

ISO 14577 establishes the method for subtracting the elastic contribution to the total displacement, thus obtaining the plastic displacements involved in the hardness definition. The cross section of the residual indentation provided in Figure 5 outlines this feature, introducing the physical meaning of the main displacement parameters:

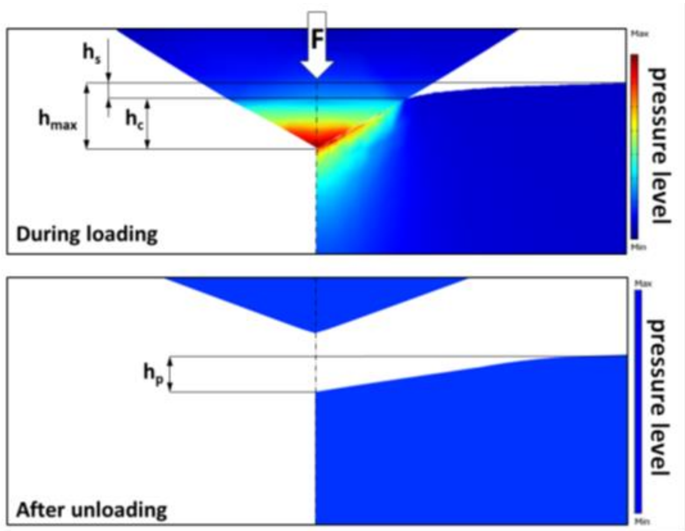

Figure 5 Cross section of an elasto-plastic indentation. hs is the displacement of the surface at the perimeter of the contact in case of sink in [57]

As can be noticed in Figure 5, the Vickers indenter actually interacts with the tested material only up to the contact depth due to the presence of sink in or pile up. The measured displacement hm is thus a function of the displacement of the tip of the indenter with respect to the original surface of the tested material (h) and of the elastic deflection due to sink-in (hs)

$$h_m = h - h_s \quad (1)$$

Since hc is measured when the load is still applied, a direct measurement is impossible. Therefore, elastic contact models are introduced in IIT.

In addition to the indentation hardness H_{IT}, many other relevant indentation parameters can be evaluated by IIT: Martens hardness HM, Martens hardness slope HMs, indentation modulus E_{IT}, indentation creep C_{IT}, indentation relaxation R_{IT}, elastic and plastic contributions of the total indentation work. In this thesis, we are mainly interested in the indentation modulus and indentation hardness.

For the specific measurement of the Young's modulus, many methods are currently available (e.g. tensile test, impulse excitation of vibration [48], atomic force microscopy) but they all show some practical drawbacks related to sample cost preparation, geometrical critical sizes or poor extraction of the elastic properties. The indentation modulus EIT measured by IIT is instead a quite close estimate of Young modulus [49].

ISO 14577-1 describes the method to extract Young modulus from the elastic displacements through the analysis of the unloading ICs. The use of the unloading portion of the indentation curves is justified assuming that a purely elastic recovery is produced when an indenter is withdrawn, at least at the beginning of the unloading (i.e. at the maximum indentation depth). The indentation modulus can be calculated using equation (3), and is comparable with young's modulus.

$$E_{IT} = \frac{1-(v_s)^2}{\frac{1}{E_{r,n}} - \frac{1-(v_i)^2}{E_i}} \quad (2)$$

Where

v_s is the Poisson's ratio of the test piece

v_i is the Poisson's ratio of the indenter (for diamond 0.07).

E_r is the reduced modulus of the indentation contact.

E_i is the modulus of indenter (for diamond 1140Gpa).

The reduced modulus of the indentation contact is determined by:

$$E_{r,0} = \frac{\sqrt{\pi}}{2C_s\sqrt{A_p(h_c)}} \quad (3)$$

Where

C_s is the compliance of the contact, i.e. dh/dF of the test force removal curve (corrected for machine compliance) evaluated at maximum test force (reciprocal of the contact stiffness)

A_p is the project contact area, the value of the indenter area function at the contact depth, h_c, defined in accordance with ISO 14577-2:2015, 4.6

Indentation hardness HIT is a measure of the resistance to permanent deformation or damage and, to a first approximation, is given by ISO 14577 in equation $H_{IT} = \frac{F_{max}}{A_p(h_c)}$ (4).

$$H_{IT} = \frac{F_{max}}{A_p(h_c)} \quad (4)$$

Where

F_{max} is the maximum applied force.

$A_p(h_c)$ is the projected (cross-sectional) area of contact between the indenter and the test piece.

Chapter 3 Experiment procedure

3.1. Sample preparation

The test samples were prepared by machining. The aluminum alloy (AA6061) tested samples were cut from the rolled sheet of testing. The thickness of the sheet is approximately 2mm. The samples were firstly cut into sheets of 25mm×25mm. Once the samples were cut, they are transferred to the factory of Maggi welding to weld with the capacitor discharge welding machine. Figure 6 is the image of the welded sample. The welding parameters are displayed in Table 4. The preloading kept constant for all the samples. Three shoots were applied to the samples with a voltage defined. The electrodes used were made in copper with brass covered at the top. During the welding, the peak of current flowing through the samples and the electrodes were measured with the coil around electrodes. In this project, the experiments are implemented with the sample Cley14.

No.	p/Mpa	Voltage/V	Ipeak/kA	Punch material	Punch configuration
Cley14	79	1800+1800+2600	102.3+101.0+132	Copper with brass upper	Convex
Cley15	79	1800+1800+2600	No*+No+132.5	Copper with brass upper	Convex
Cley16	79	1800+1800+2600	103.6+no++132.5	Copper with brass upper	Convex

Table 4 Parameters of welding (*No means the current peak was not measured)

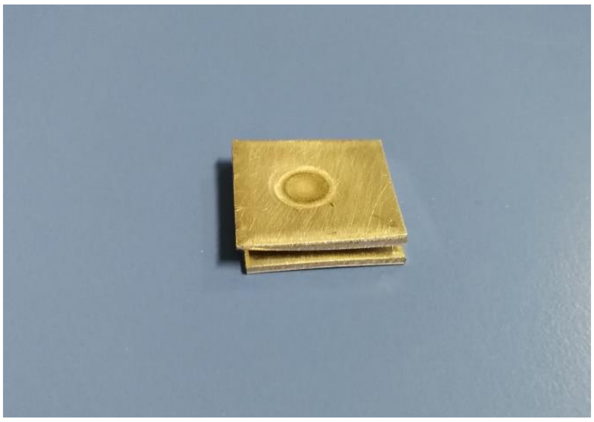

Figure 6 Welded sample

3.2. Metallographic analysis

Firstly, the welded sample was cut near the center of the welding zone and both parts are mounted into the resin. Figure 7 shows the sample after the experiments. Then the section of the welding zone is polished finishing with 1µm crystalline suspension.

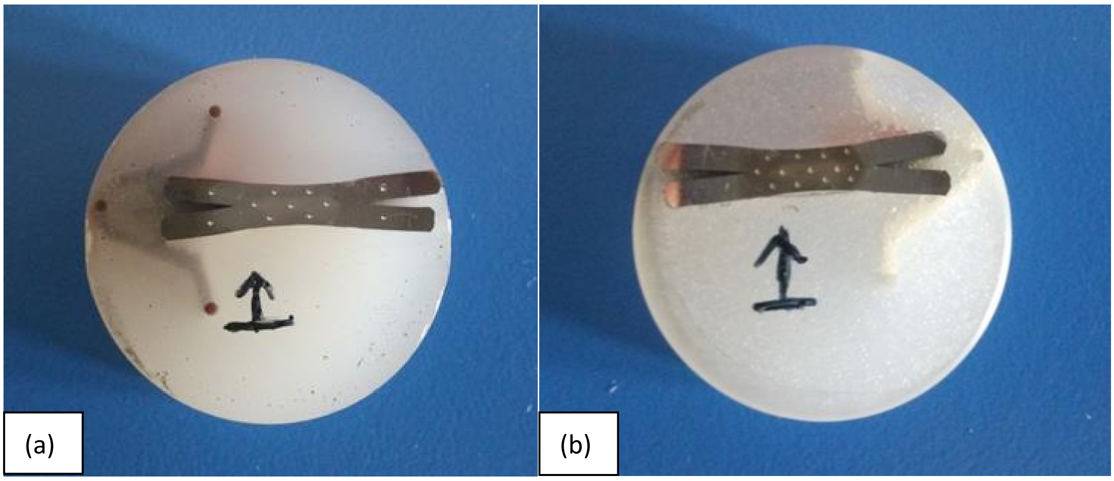

Figure 7 (a)(Larger part) sample 1. (b) (Smaller part) sample 2.

Figure 8 LEICA DMI 3000M optical microscope

After the samples were polished well, the surface was etched in order to observe the microstructure both of the base material and the welding zone. The etch agent were Keller, which is a mixture of nitric acid (HNO_3), hydrochloric acid (HCl), and hydrofluoric acid (HF), and Weck, which is a mixture of sodium hydroxide (NaOH) and potassium permanganate ($KMnO_4$) solution. Two procedures of etching condition were applied: the first was 45s of Keller+4s of Weck; the second was 45s of Keller+4s of Weck+3s of Keller (Figure 9). With the first etching condition, it showed well the grain boundary of sample, however the observation of microstructure within the grains was interfered negatively by the color introduced by the $KMnO_4$ (figure 7a). For this reason, the Keller is applied again, demonstrated by the second etching condition, in order to eliminate the effect of KMnO4 (figure 7b).

Finally, the etched samples were observed on the optical microscopy (Figure 8) with different magnifications. The figures were acquired at the interested zones and at the base material in order to understand the phenomenon happened due to welding.

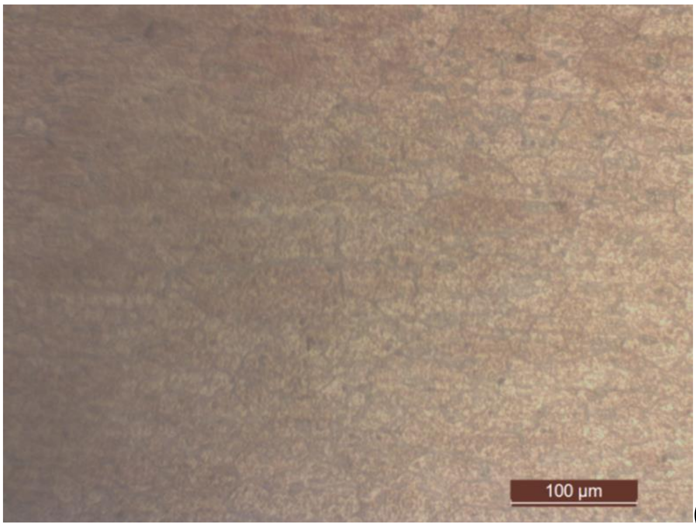

(a)

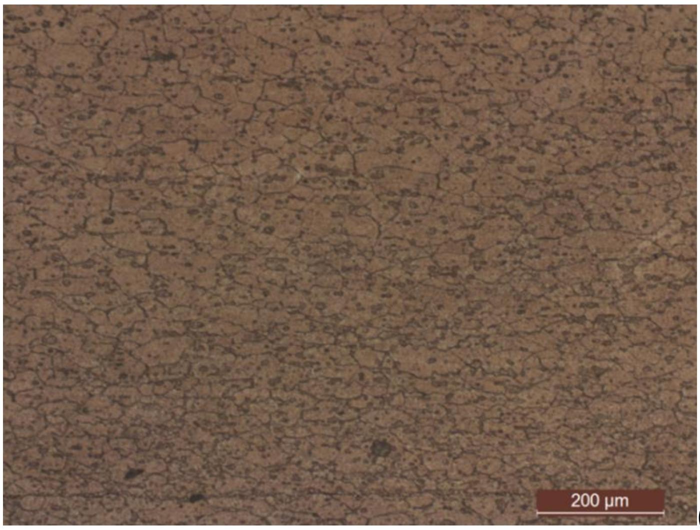

(b)

Figure 9 Microstructure with etching of (a) Keller+Weck (b) Keller+Weck+Keller

3.3. Macro instrumented indentation test

The instrumented indentation test is implemented with a macro-indenter prototype device (OMAG SR HU 09) (Figure 10). The indentations are impressed in sequence along the welding line namely, at the welding line, inside the heat affected zone and in the base material (Figure 11). Each indentation consists of ten load-hold-unload cycles. The indentation parameters, such as the imposed load, loading time, holding time and unloading time, are defined in Table 5. The recorded quantities are managed OMAG software and the output is finally converted into indentation curves with Matlab.

Figure 10 OMAG SR HU 09 macro-indenter prototype

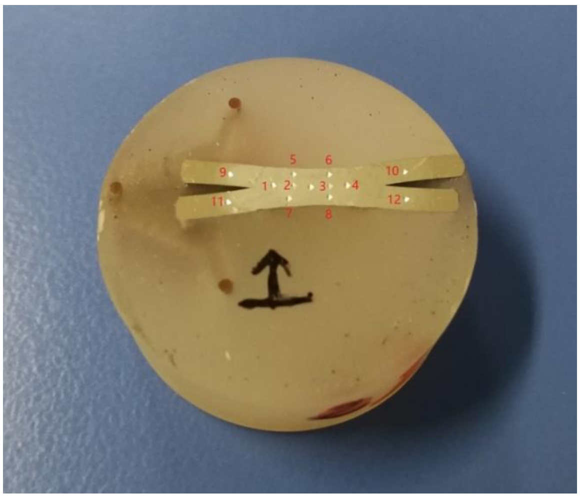

Figure 11 Sequence of indentation on sample 1

Load/N	Loading time/s	Holding time/s	Unloading time/s	Cycles
100	30	30	10	10

Table 5 Indentation parameters

Chapter 4 Result and discussion

4.1. Microstructure analysis

Micrographs, acquired from the optical microscope, were analysed over a range of magnifications display the microstructure in the base material and the in the welding zone.

Figure 12 shows the microstructure of the base material. The small and large size particles are distributed randomly in the aluminum matrix. These particles are intermetallic based on Al and impurity elements (Mg, Si and Fe).

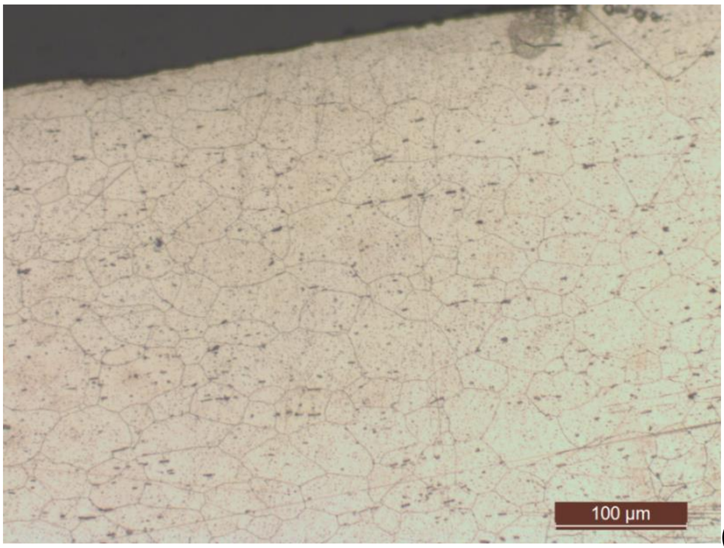

(a)

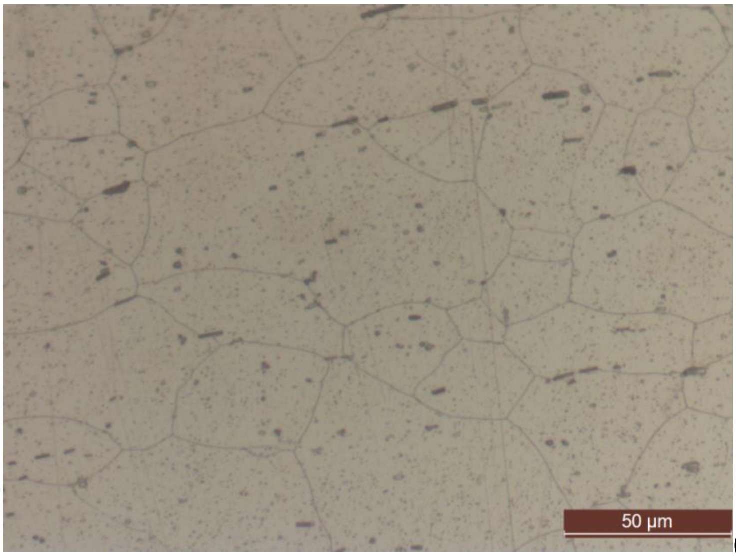

(b)

Figure 12 Micro structure of base material at (a) x200 and (b) x500 magnification.

Figure 13 shows the overview of the microstructure in the welding spot area. Close to the welding line, a special refined microstructure caused by the impulsive heating during the capacitor discharge welding, is visible.

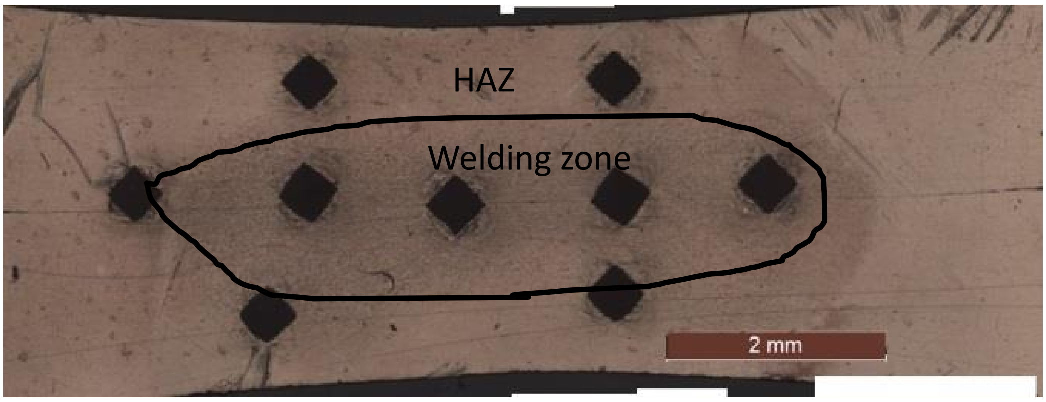

Figure 13 Overview of welding zone

Figure 14 shows the microstructure around the welding line. An apparent welding line is visible between welded sheets. During welding the material was not melted and did not form any fusion zone. Many 'spot features', evidenced by the 'Keller+Weck+Keller' etching, were observed in the welding zone, and their density decreased gradually outwards from the welding line. This is because at the interface of two sheets the contact resistance at the interface of two sheets is much higher than that in other areas of the sample and, thus dissipated a highly concentrated heat. As a result, the 'spot features' originated by the intensive heating exhibited a high density near the welding line than near the surface of the sheets.

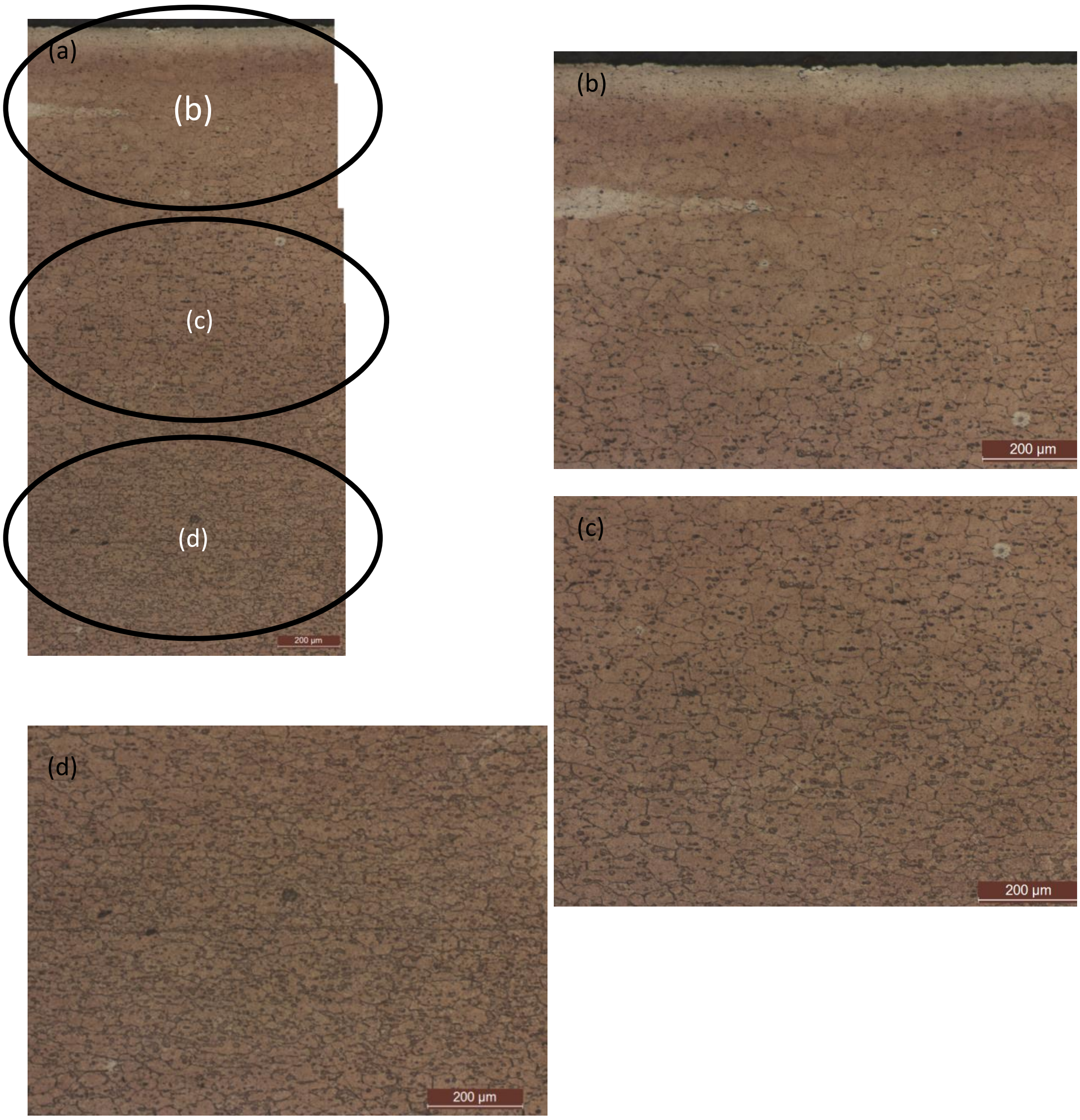

Figure 14 Micro structure a) of a chosen section b) near surface c) in the middle d) near the welding line

Figure 15 (a-b) shows the microstructure (x500) at the welding line. The finer recrystallized grains (5 to 10µm average grain size) formed at the welding line, which are responsible of the bonding of the two sheets. A few pores at the welding line are observed as well.

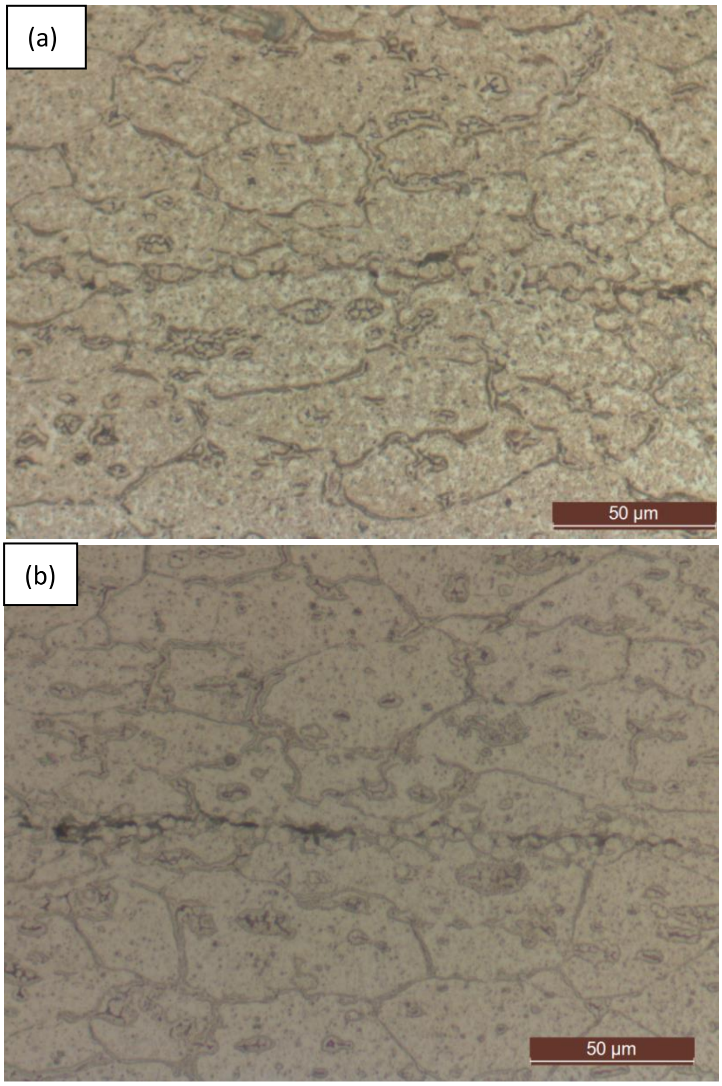

Figure 15 Detail of welding line

The electron dispersive spectra (EDS) analysis was carried out with the scanning electron microscope at two points, namely near the welding line and away from the welding line but in the welding zone, to understand recrystallization phenomena during solid state CDW.

The EDS 1 and EDS 2 are done across a peculiar ‘microstructure feature’ near the welding line (Figure 16 (a)-(c)). EDS 1 (Figure 17) was selected over the boundary of the feature and EDS2 (Figure 18) was selected outside the feature. EDS 1 demonstrates that it contains 0.80% of Fe which is absent at point of EDS 2. Furthermore, the concentration of Mn and Si is higher at the point of EDS 1 than EDs 2, while it presents a high amount of carbon at the point of EDS 2 (although the latter element is not accurately accounted for by EDS).

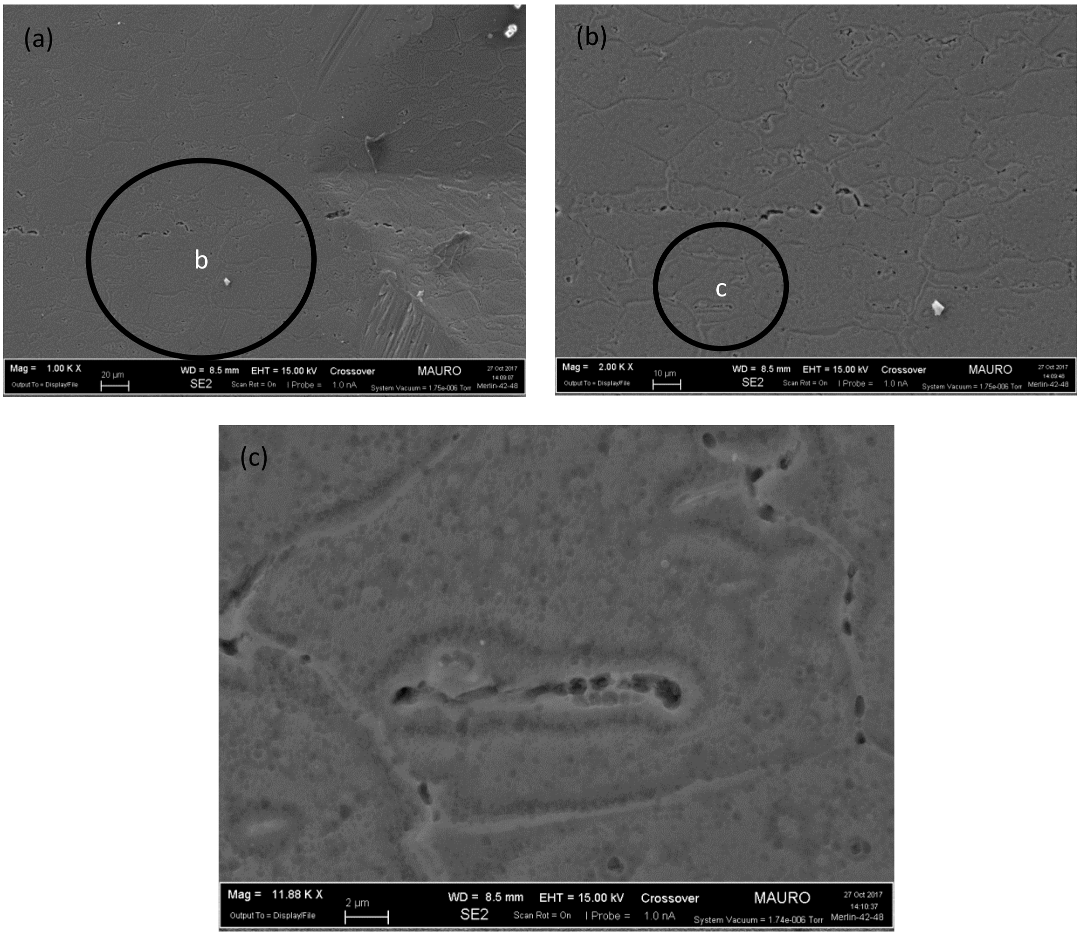

Figure 16 SEM graph for SDA 1&2

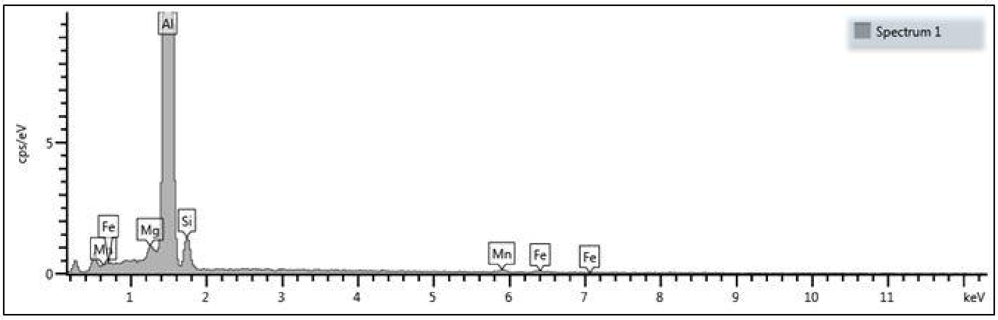

Spectrum 1

Element	Wt%	Wt% Sigma
Mg	0.68	0.08
Al	92.83	0.34
Si	4.50	0.19
Mn	1.19	0.19
Fe	0.80	0.21
Total:	100.00	

AA6061

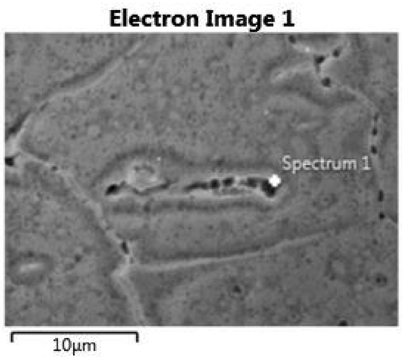

Figure 17 Result of SDA 1

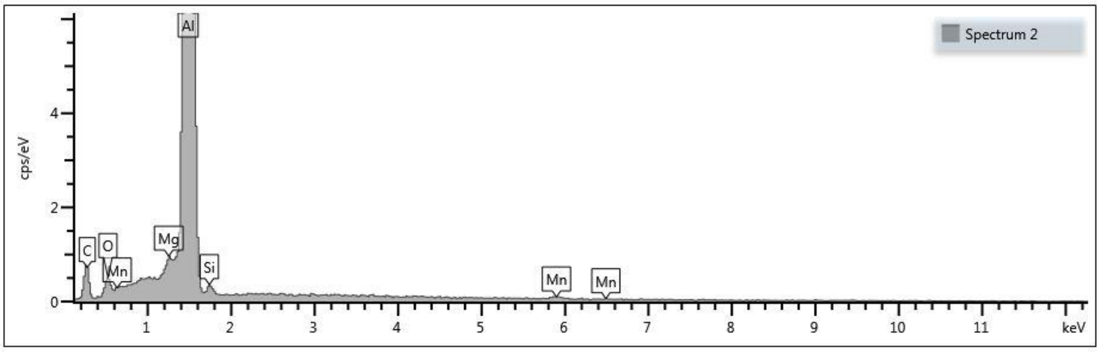

Spectrum 2

Element	Wt%	Wt% Sigma
C	18.77	0.61
O	2.26	0.18
Mg	0.34	0.05
Al	77.68	0.61
Si	0.49	0.06
Mn	0.46	0.10
Total:	100.00	

AA6061

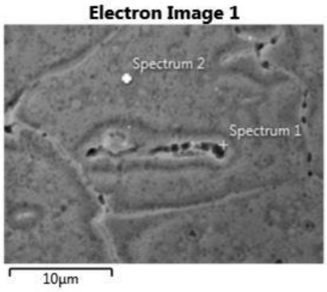

Figure 18 Result of SDA 2

EDS 3 is done at distance approximately 250μm from the welding line (Figure 19 (a)-(c)) inside another peculiar microstructure feature (Figure 20). It shows the presence of Fe, Mn, Si and C. The result illustrates that these features are characterized by the prior presence of a sort of low melting point Fe-based micro-constituent in the alloy, so that undesirable liquid phase transformation occur during solid state CDW. The presence of Fe and C in sufficient amount is compatible with a secondary (i.e., recycled) alloy.

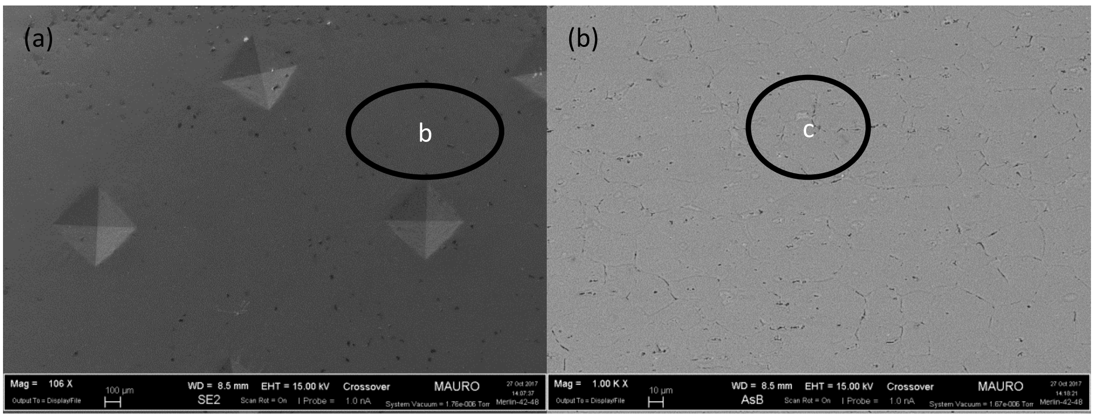

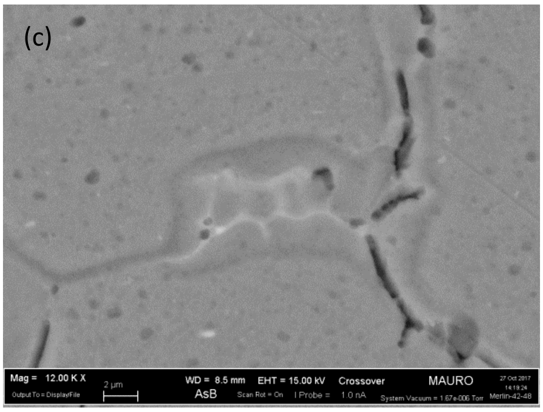

Figure 19 SEM graph for SDA 3

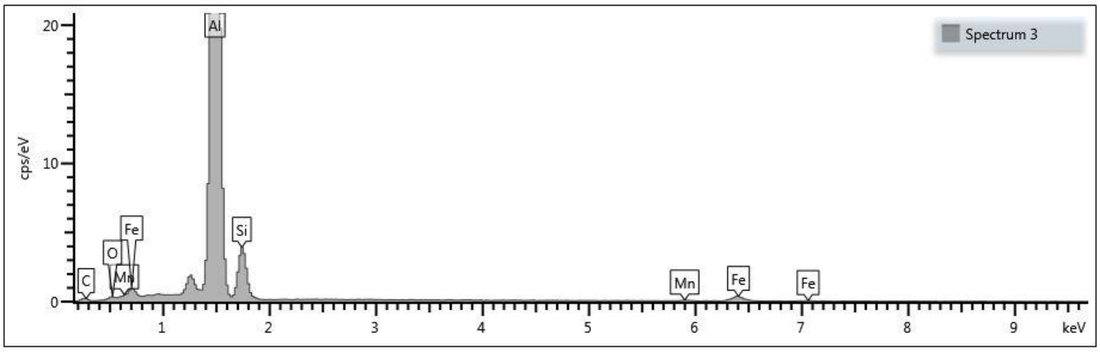

Spectrum 3

Element	Wt%	Wt% Sigma
C	6.89	0.68
O	1.49	0.21
Al	75.91	0.63
Si	10.62	0.20
Mn	0.52	0.13
Fe	4.57	0.23
Total:	100.00	

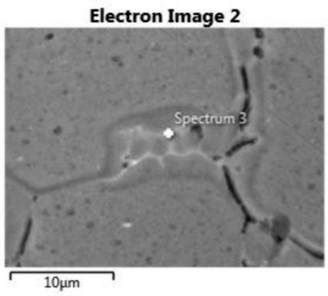

AA6061

Figure 20 Result of SDA 3

4.2. Macroinstrumented indentation test

The macroinstrumented indentation test is implemented on the polished surfaces of the sample. Figure 21 shows the sequence of indents, a number of four indents are at the welding line, four are in the heat affected zone (HAZ, away from the welding line), and four are in the base material. Every indentation consists of 10 cycles.

Figure 22 show the maximum displacement of indents. The indentation 1 is out of the welding zone core although it is at the welding line (see Figure 13), as a result the value of maximum displacement (as well as h_c and h_p) here is lower than those in the welding zone. Figure 23 shows the average value of maximum displacement by cycles. The indentation properties at both the welding line and HAZ are approximately 17% and 9% respectively higher than those in the base material.

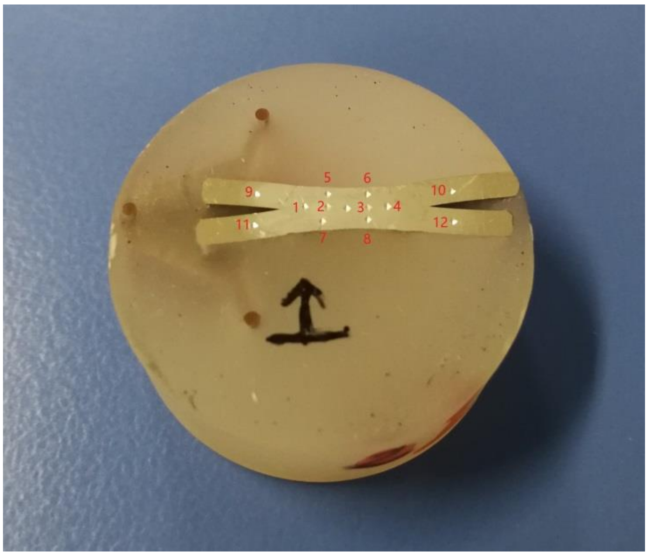

Figure 21 Sequence of indents on sample1

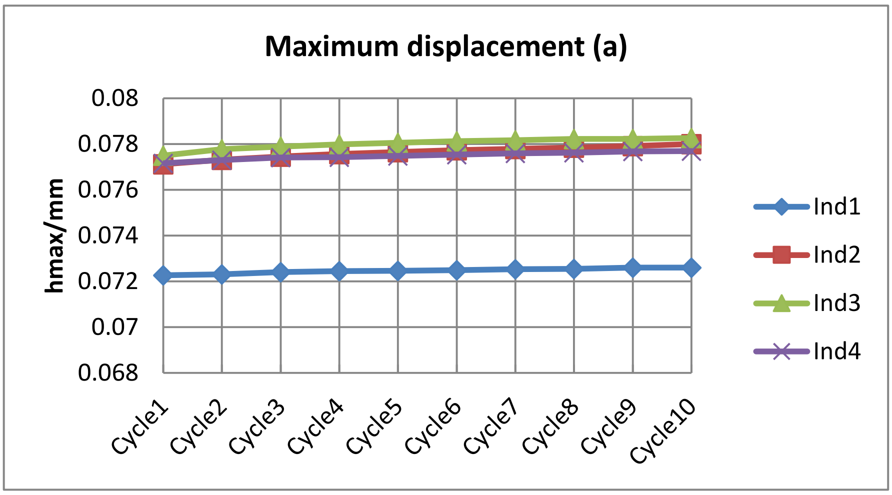

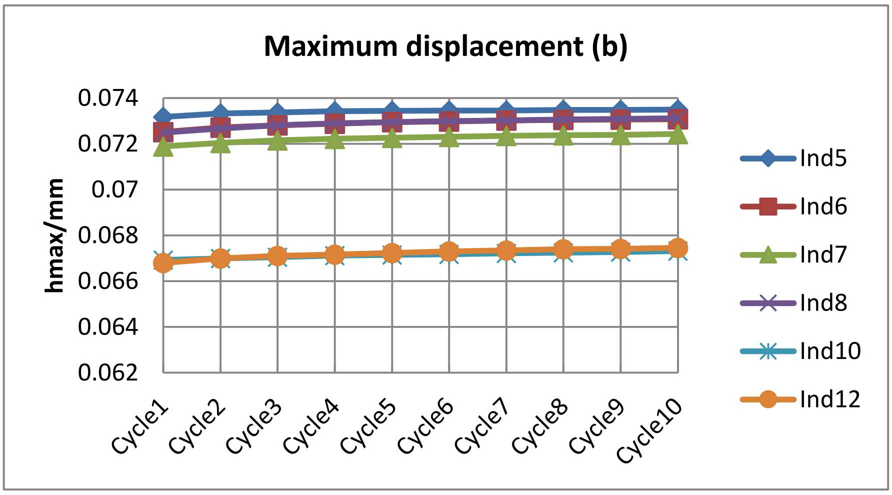

Figure 22 Maximum displacement upon indentations (a) at welding line (b) in HAZ and base material

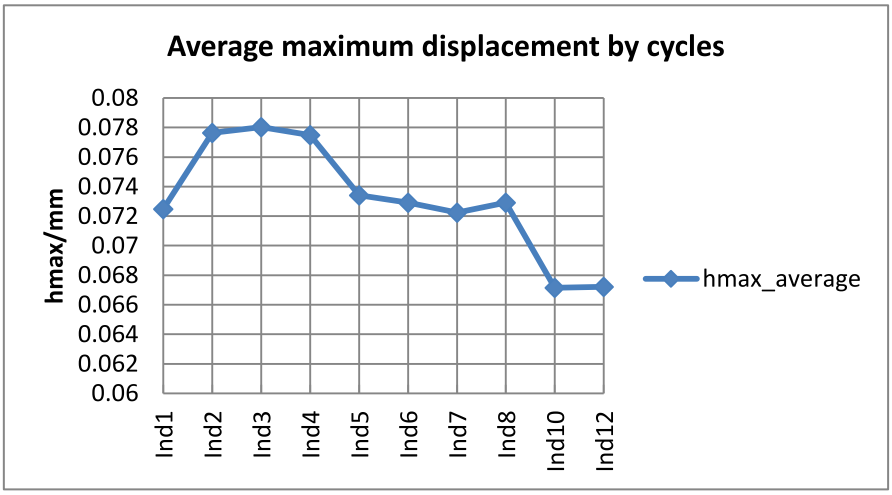

Figure 23 Average values of maximum displacement over cycles

Figure 24 and Figure 25 show the values of contact depth, and Figure 26 and Figure 27 show the values of plastic depth upon indentations. These two groups of data show similar behavior with respect to the aforesaid maximum displacement.

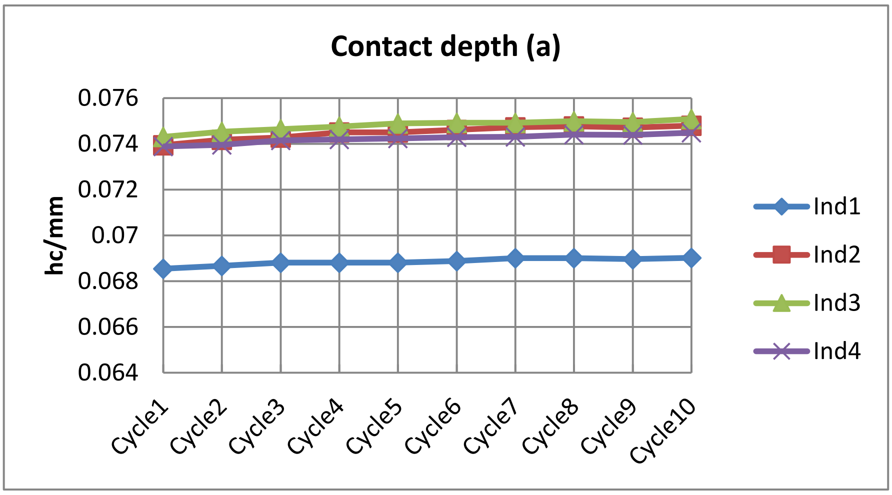

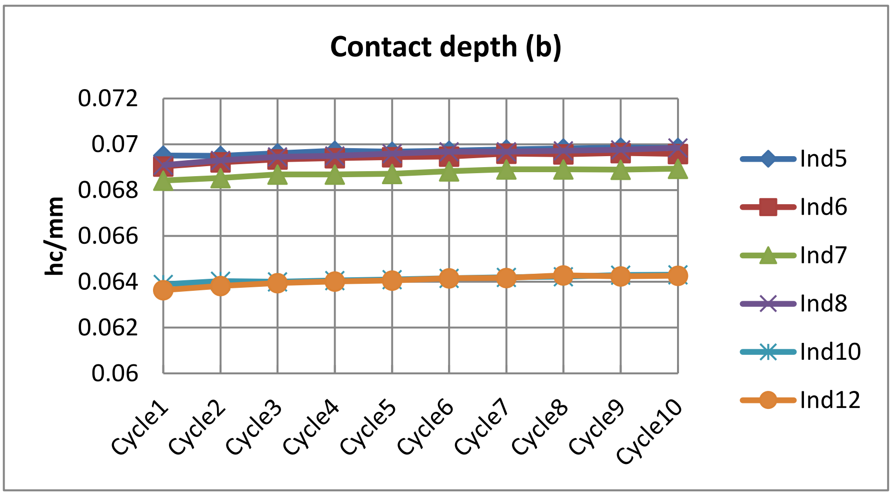

Figure 24 Contact depth upon indentations (a) at welding line (b) in HAZ and base material

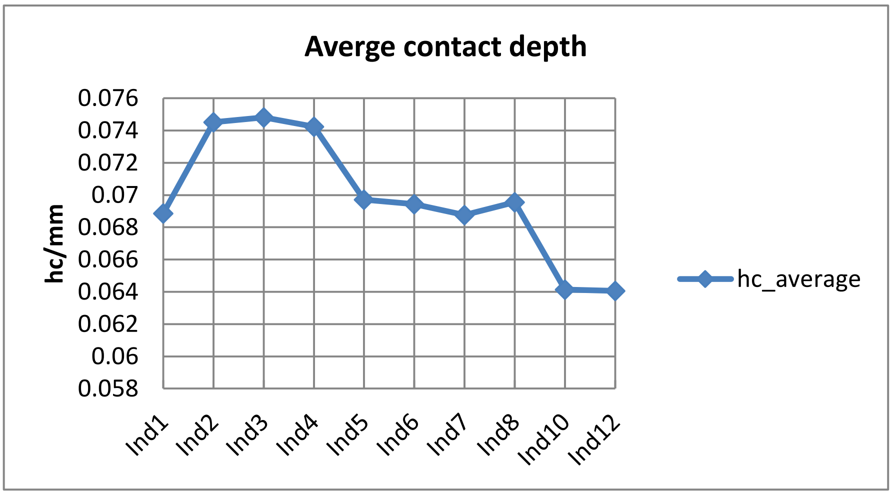

Figure 25 Average values of contact depth over cycles

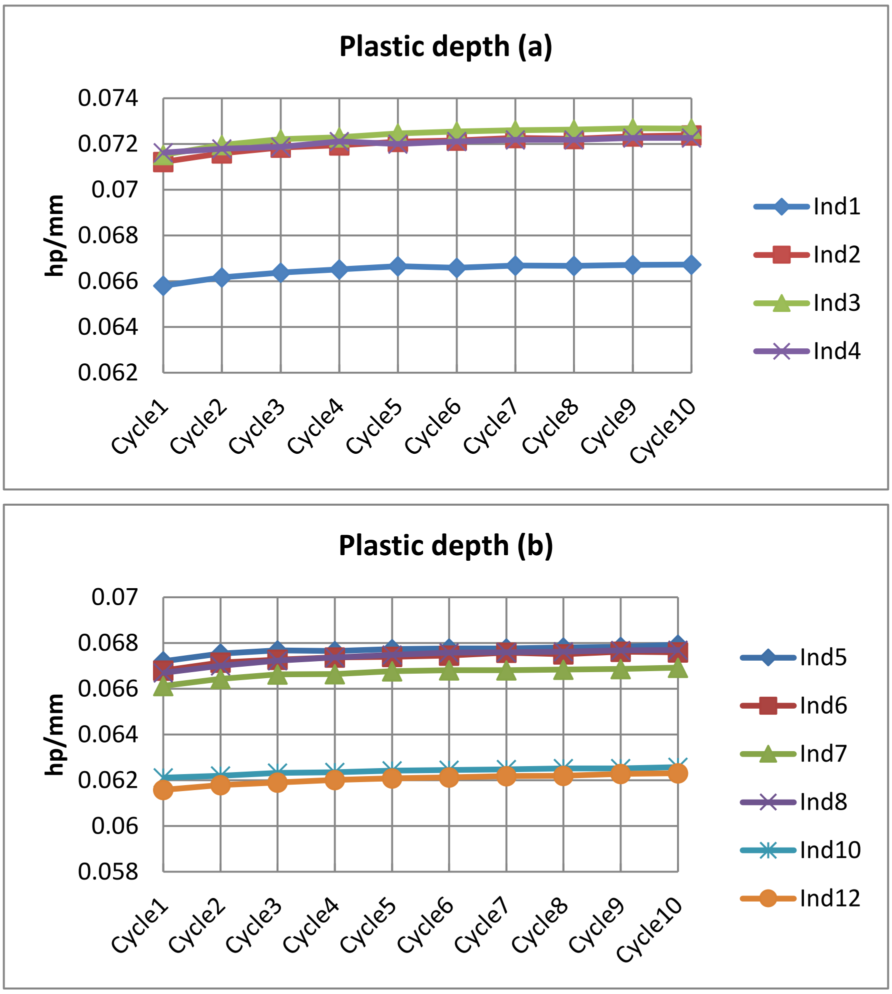

Figure 26 Plastic depth upon indentations (a) at welding line (b) in HAZ and base material

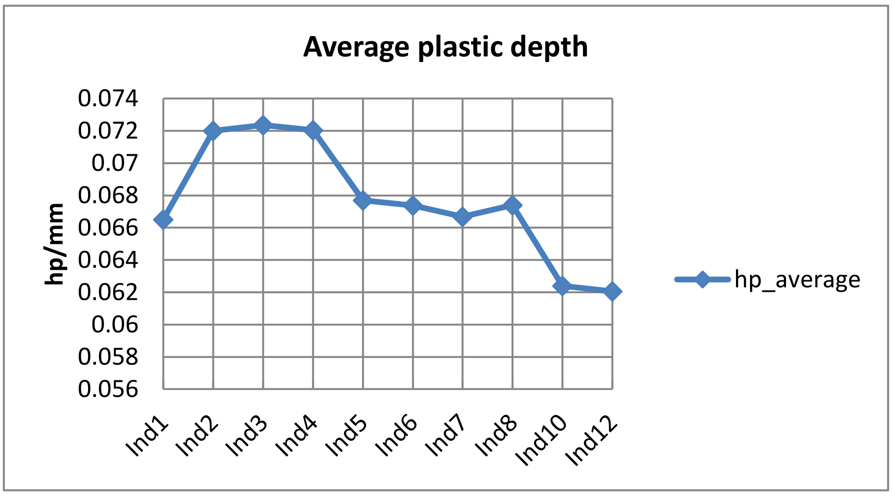

Figure 27 Average values of plastic depth over cycles

As expected, the material in the welding zone and HAZ is softened as is documented by both the indentation modulus (Figure 28) and indentation hardness (Figure 29), while the property in the welding zone, whose indentation hardness is lower lower than HAZ, shows a more softening and plasticity (Figure 30). This additional plasticity is attributed to the recrystallization structure shown by the fine grains about the welding line. These grains which are about 5 to 10µm in diameter, can be almost considered as spheres. It is believed that during indentation, these grains tend to plastically deform by relative sliding rather than normally strain-hardening by regular dislocation dynamics. This behavior might be associated to a unique superplastic behavior of the solid state welded region which, among others, undergoes to some extent precipitation hardening (aging) after welding. This unique grain boundary sliding mechanism has been observed 200µm away from the welding line. However, the larger the distance is from the welding line, the larger the influence of dislocation accounts for the plasticity with respect to the super-plasticity. In such remote regions as well as in HAZ, higher hardness is observed upon indentation.

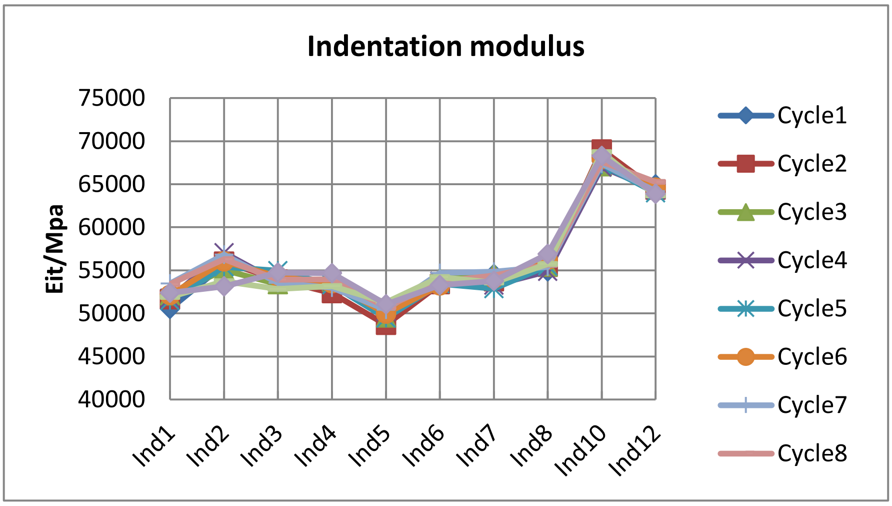

Figure 28 Indentation modulus

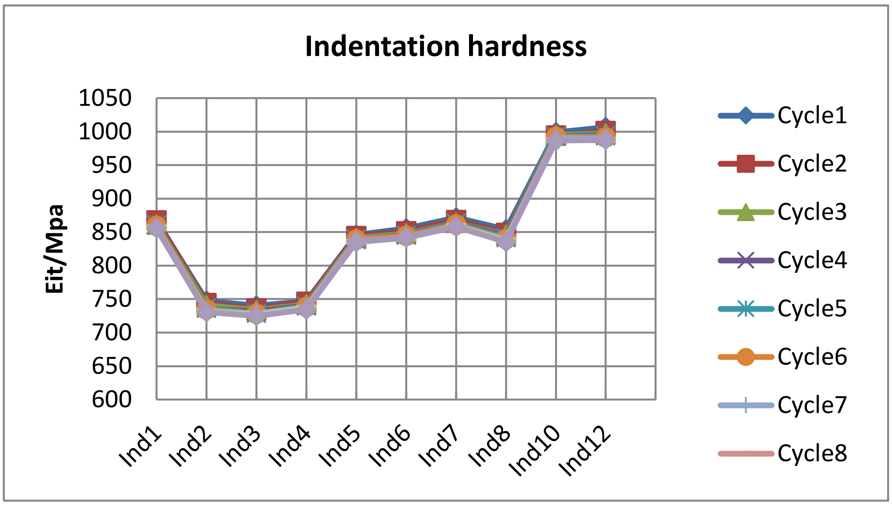

Figure 29 Indentation hardness

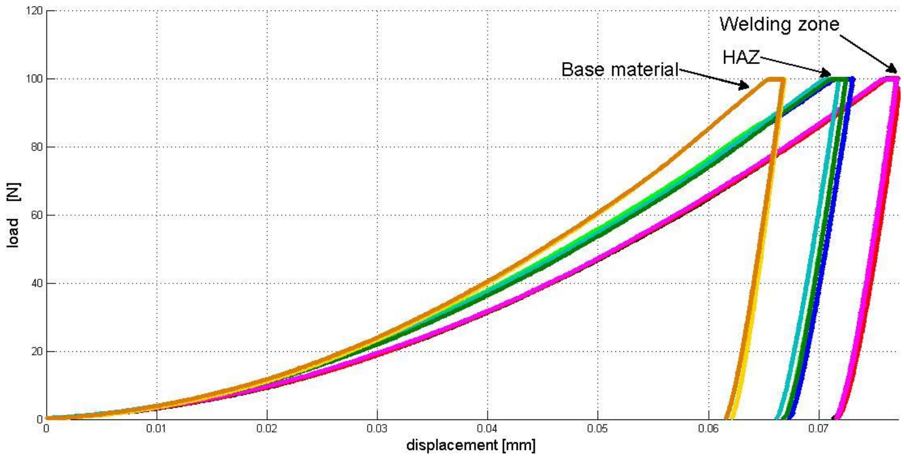

Figure 30 Indentation curves

Chapter 5 Conclusion

Aluminum alloys have great potentials for weight saving and are receiving increasing attention in the automotive industry to fulfill effective strategies of fuel efficiency and low emissions in the atmosphere. Capacitor discharge welding, on its own, reveals as a viable assembly technology of aluminum alloy sheets to be used in the automotive industry. This thesis presents an experimental method to characterize the morphological and mechanical properties of monolithic welding of 6061 aluminum alloy.

The metallographic analysis illustrates the morphological change of the material during the welding process. A certain recrystallization occurred at the welding line. Undesirable liquid phase transformation of eutectic regions was observed due to low initial quality of the alloy, mainly attributed to the presence of Fe.

The macro-instrumented indentation test is a valuable means to characterize the mechanical properties of the welding joints in so narrow regions while permitting a correlation with conventional tensile test properties. However, the CDW of AA6061 causes some softening in the welding region, although the increased refinement of the HAZ is greatly beneficial from the fracture toughness point of view.

To establish some standards for testing and welding in the automotive sector, further researches are required. The change of material properties under various welding parameters should be tested as well.

Reference

[1] Kim HC, Wallington TJ (2013) Life-cycle energy and greenhouse gas emission benefits of light weighting in automobiles: review and harmonization. Environ Sci Technol 47(12):6089–6097

[2] Humpenöder F, Popp A, Stevanovic M, Müller C, Bodirsky BL, Bonsch M, Dietrich JP, Lotze-Campen H, Weindl I, Biewald A (2015) Land-use and carbon cycle responses to moderate climate change: implications for land-based mitigation? Environ Sci Technol

[3] Modaresi R, Pauliuk S, Løvik AN, Müller DB (2014) Global carbon benefits of material substitution in passenger cars until 2050 and the impact on the steel and aluminum industries. Environ Sci Technol 48(18):10776–10784

[4] Das S (2014) Life cycle energy and environmental assessment of aluminum-intensive vehicle design. SAE Int J Mater Manuf 7(2014-01-1004):588–595

[5] Kulekci MK (2008) Magnesium and its alloys applications in automotive industry. Int J Adv Manuf Technol 39(9-10):851–865

[6] Medraj M, Parvez A (2007) Analyse the importance of magnesium-aluminium-strontium alloys for more fuel-efficient automobiles. Automotive:45–47

[7] Association EA (2008) Aluminium in cars. European Aluminium Association,

[8] Sun M, Niknejad S, Gao H, Wu L, Zhou Y (2016) Mechanical properties of dissimilar resistance spot welds of aluminum to magnesium with Sn-coated steel interlayer. Mater Des 91:331–339

[9] Ambroziak A, Korzeniowski M (2010) Using resistance spot welding for joining aluminium elements in automotive industry. Arch Civ Mech Eng 10(1):5–13

[10] Automotive Trends in Aluminum, The European perspective: part one. http://www.totalmateria.com/Article135.htm Accessed 12 Dec 2015

[11] Rodriguez R, Jordon J, Allison P, Rushing T, Garcia L (2015) Microstructure and mechanical properties of dissimilar friction stir welding of 6061-to-7050 aluminum alloys. Mater Des 83:60–65

[12] Liu J, Rao Z, Liao S, Wang P-C (2014) Modeling of transport phenomena and solidification cracking in laser spot bead-onplate welding of AA6063-T6 alloy. Part I—the mathematical model. Int J Adv Manuf Technol 73(9-12):1705–1716

[13] Qiu R, Zhang Z, Zhang K, Shi H, Ding G (2011) Influence of welding parameters on the tensile shear strength of aluminum alloy joint welded by resistance spot welding. J Mater Eng Perform 20(3):355–358

[14] Karimi M, SedighiM, Afshari D (2015) Thermal contact conductance effect in modeling of resistance spot welding process of aluminum alloy 6061-T6. Int J Adv Manuf Technol 77(5-8):885– 895

[15] Han L, Thornton M, Shergold M (2010) A comparison of the mechanical behaviour of self-piercing riveted and resistance spot welded aluminium sheets for the automotive industry. Mater Des 31(3):1457–1467

[16] Han L, Thornton M, Li D, ShergoldM(2011) Effect of governing metal thickness and stack orientation on weld quality and mechanical behaviour of resistance spot welding of AA5754 aluminium. mMater Des 32(4):2107–2114

[17] ZhangY, Li Y, Luo Z, Yuan T, Bi J,Wang ZM,Wang ZP, Chao YJ (2016) Feasibility study of dissimilar joining of aluminum alloy 5052 to pure copper via thermo-compensated

resistance spot welding. Mater Des 106:235–246
[18] Shi Y, Guo H (2013) Fatigue performance and fatigue damage parameter estimation of spot welded joints of aluminium alloys 6111 - T4 and 5754. Fatigue Fract Eng Mater Struct 36(10):1081 - 1090
[19] HaoM, Osman K, Boomer D, Newton C (1996) Developments in characterization of resistance spot welding of aluminum. Weld J Incl Weld Res Suppl 75(1):1–4
[20] Cho Y, Hu S, LiW (2003) Resistance spot welding of aluminium and steel: a comparative experimental study. Proc Inst Mech Eng B J Eng Manuf 217(10):1355–1363
[21] Luo Z, Ao S, Chao YJ, Cui X, Li Y, Lin Y (2015) Application of pre-heating to improve the consistency and quality in AA5052 resistance spot welding. J Mater Eng Perform 24(10):3881–3891
[22] Cui LH,Qiu RF, ShiHX, ZhuYM(2014) Resistance spotwelding between copper coated steel and aluminum alloy. Appl Mech Mater 675:19–22
[23] Florea R, Solanki K, Bammann D, Baird J, Jordon J, Castanier M (2012) Resistance spot welding of 6061-T6 aluminum: failure loads and deformation. Mater Des 34:624–630
[24] 2015 North American light vehicle aluminum content study: executive summary http://www.drivealuminum.org/researchresources/PDF/Research/2014/2014-ducker-report. Accessed 12 Dec 2015
[25] Srinivas M. Patnaik (1996) Development of an automated Capacitor Discharge Welding System
[26] Wilson ,R.D., "Explore the potential of capacitor discharge welding", Advanced Materals and Processes, vol. 145, no. 6, pp. 93-94, 1994
[27] Li YB, Wei ZY, Li YT, Shen Q, Lin ZQ (2013) Effects of cone angle of truncated electrode on heat and mass transfer in resistance spot welding. Int J Heat Mass Transf 65:400–408
[28] Hamidinejad SM, Kolahan F, Kokabi AH (2012) The modeling and process analysis of resistance spot welding on galvanized steel sheets used in car body manufacturing. Mater Des 34:759–767
[29] Hayat F (2011) The effects of the welding current on heat input, nugget geometry, and the mechanical and fractural properties of resistance spot welding on Mg/Al dissimilar materials. Mater Des 32(4):2476–2484
[30] Florea R, Bammann D, Yeldell A, Solanki K, Hammi Y (2013) Welding parameters influence on fatigue life and microstructure in resistance spot welding of 6061-T6 aluminum alloy. Mater Des 45:456–465
[31] Pouranvari M, Marashi S (2013) Critical review of automotive steels spot welding: process, structure and properties. Sci Technol Weld Join 18(5):361–403
[32] Manladan S, Yusof F, Ramesh S, Fadzil M (2016) A review on resistance spot welding of magnesium alloys. Int J Adv Manuf Technol:1-21. doi: 10.1007/s00170-015-8258-9
[33] Basic Knowledge of Capacitive Discharge Spot Welder (CD Welder) Spot Welders, http://www.batteryspace.com/prod-specs/5997.htm
[34] Kissell, J.R., Ferry, R.L. (2002) "Aluminum Structures: A Guide to Their Specifications and Design." New York: John Wiley & Sons, Inc
[35] D.J. Chakrabarti, Alcoa Technical Center, Alcoa Center, PA 15069, USA, Precipitation in Al-Mg-Si-Cu Alloys and the Role of the Q Phase and its Precursors, The Minerals, Metals, and Materials Society, 1998

[36] Wei PS, Wu TH, Chen LJ (2013) Joint quality affected by electrode contact condition during resistance spot welding. IEEE Trans Compon Pack Manuf Technol 3(12):2164–2173
[37] Liu L, Feng J, Zhou Y (2010) 18 - Resistance spot welding of magnesium alloys. In: Liu L (ed) Welding and joining of magnesium alloys. Woodhead Publishing, pp 351–367e
[38] Qiu RF, Satonaka S, Iwamoto C (2009) Mechanical properties and microstructures of magnesium alloy AZ31B joint fabricated by resistance spot welding with cover plates. Sci Technol Weld Join 14(8):691–697
[39] Charde N, Yusof F, Rajkumar R (2014) Material characterizations of mild steels, stainless steels, and both steel mixed joints under resistance spot welding (2-mm sheets). Int J Adv Manuf Technol 75(1-4):373–384
[40] Wang Y, Mo Z, Feng J, Zhang Z (2007) Effect of welding time on microstructure and tensile shear load in resistance spot welded joints of AZ31 Mg alloy. Sci Technol Weld Join 12(8):671–676
[41] Zhang H, Senkara J (2011) Resistance welding: fundamentals and applications. CRC Press
[42] Williams N, Parker J (2004) Review of resistance spot welding of steel sheets part 1modelling and control of weld nugget formation. Int Mater Rev 49(2):45–75
[43] James P, Chandler H, Evans J, Wen J, Browne D, Newton C (1997) The effect of mechanical loading on the contact resistance of coated aluminium. Mater Sci Eng A 230(1):194–201
[44] Crinon E, Evans J (1998) The effect of surface roughness, oxide film thickness and interfacial sliding on the electrical contact resistance of aluminium. Mater Sci Eng A 242(1):121–128
[45] Cagliero, R (2016). Macro instrumented indentation test for structural materials: experimental and numerical methods. PhD thesis
[46] Doerner MF, Nix WD. A method for interpreting the data from depth-sensing indentation instruments. Journal of Materials Research 1986; 1(4):601-609.
[47] Stillwell NA, Tabor D. Elastic recovery of conical indentation. Proceedings of the Royal Society of London 1961; 78:169-179.
[48] ASTM E1876 - 09. Standard Test Method for Dynamic Young's Modulus, Shear Modulus, and Poisson's Ratio by Impulse Excitation of Vibration.
[49] Fischer-Cripps AC. Nanoindentation. 2nd ed. New York: Springer; 2003.

Appendix: Indentation test data sheets

Maximum displacement

hmax/mm	Ciclo 1	Ciclo2	Ciclo3	Ciclo4	Ciclo5	Ciclo6	Ciclo7	Ciclo8	Ciclo9	Ciclo10
indentazione1	0.072269	0.072309	0.072406	0.072453	0.072469	0.072494	0.072541	0.072549	0.072605	0.072605
indentazione2	0.07712	0.077319	0.077463	0.077575	0.077655	0.077735	0.077791	0.077855	0.077918	0.077998
indentazione3	0.077495	0.077775	0.077894	0.077991	0.078054	0.078126	0.078166	0.078223	0.078223	0.078263
indentazione4	0.077161	0.077305	0.077417	0.077433	0.077489	0.077545	0.077593	0.077625	0.077681	0.077689
indentazione5	0.073174	0.073324	0.073372	0.073429	0.073445	0.073461	0.07346	0.073477	0.073485	0.073492
indentazione6	0.072524	0.072717	0.072812	0.072884	0.072948	0.072974	0.07302	0.073045	0.07306	0.073076
indentazione7	0.071886	0.072039	0.07215	0.072222	0.072263	0.072303	0.072358	0.072374	0.07239	0.072431
indentazione8	0.072493	0.072678	0.072813	0.072893	0.072949	0.072989	0.073029	0.07307	0.073093	0.073126
indentazione9	0.067153	0.067289	0.067402	0.067465	0.06753	0.067578	0.067633	0.067642	0.067673	0.067682
indentazione10	0.066921	0.067002	0.067057	0.067129	0.067145	0.067177	0.067225	0.067249	0.067273	0.06732
indentazione11	0.067337	0.067505	0.067633	0.067721	0.067793	0.067841	0.067898	0.067961	0.067986	0.068034
indentazione12	0.066802	0.066993	0.067105	0.067169	0.067233	0.067305	0.067345	0.067409	0.067417	0.067457

Plastic depth

hp/mm	Ciclo 1	Ciclo2	Ciclo3	Ciclo4	Ciclo5	Ciclo6	Ciclo7	Ciclo8	Ciclo9	Ciclo10
indentazione1	0.065803	0.066171	0.066387	0.066523	0.066667	0.066595	0.066683	0.066675	0.066715	0.066731
indentazione2	0.071223	0.071599	0.071854	0.071942	0.072094	0.072158	0.072262	0.07223	0.072334	0.072374
indentazione3	0.071527	0.071966	0.072206	0.072294	0.072462	0.07255	0.072598	0.07263	0.072694	0.072678
indentazione4	0.071623	0.071799	0.071878	0.072118	0.071998	0.07211	0.072182	0.07219	0.07227	0.07227
indentazione5	0.067202	0.067546	0.067682	0.067658	0.06773	0.067762	0.067762	0.067802	0.067834	0.06793
indentazione6	0.066803	0.067146	0.067274	0.06737	0.067402	0.067458	0.067578	0.067514	0.067626	0.067602
indentazione7	0.066123	0.066443	0.066627	0.066651	0.066771	0.066819	0.066811	0.066843	0.066874	0.06693
indentazione8	0.066707	0.06701	0.067234	0.067378	0.06749	0.067578	0.067594	0.067626	0.067682	0.067698
indentazione9	0.060544	0.060903	0.061063	0.061223	0.061271	0.061335	0.061423	0.061415	0.061455	0.061471
indentazione10	0.06211	0.062206	0.062326	0.06235	0.062422	0.062454	0.062478	0.062526	0.062526	0.062574
indentazione11	0.06004	0.06044	0.060687	0.060879	0.061023	0.061127	0.061175	0.061239	0.061367	0.061391
indentazione12	0.061583	0.061791	0.061911	0.062022	0.062086	0.062134	0.06219	0.062206	0.062278	0.062318

Contact depth

hc/mm	Ciclo 1	Ciclo2	Ciclo3	Ciclo4	Ciclo5	Ciclo6	Ciclo7	Ciclo8	Ciclo9	Ciclo10
indentazione1	0.068555	0.068678	0.068814	0.06882	0.068815	0.068883	0.069012	0.069016	0.068974	0.069021
indentazione2	0.073953	0.074188	0.074277	0.074504	0.074509	0.074612	0.074728	0.074773	0.074713	0.074797
indentazione3	0.074303	0.074529	0.074643	0.074755	0.074897	0.074927	0.07492	0.074996	0.074957	0.075092
indentazione4	0.073887	0.073958	0.074149	0.0742	0.074239	0.074302	0.074311	0.074401	0.074393	0.074494
indentazione5	0.069511	0.069505	0.069613	0.06972	0.069685	0.069725	0.069782	0.069822	0.069867	0.069854
indentazione6	0.069034	0.069217	0.06935	0.069406	0.069449	0.069476	0.069603	0.069565	0.069623	0.069587
indentazione7	0.068417	0.068537	0.068691	0.068694	0.068718	0.068827	0.068913	0.068911	0.068891	0.068934
indentazione8	0.069091	0.069308	0.069453	0.069494	0.069597	0.069678	0.069679	0.069728	0.069759	0.069853
indentazione9	0.062975	0.063176	0.063294	0.063349	0.063397	0.063463	0.063598	0.06361	0.063597	0.063663
indentazione10	0.063892	0.064036	0.064011	0.064065	0.064109	0.064161	0.064195	0.064228	0.064302	0.064319
indentazione11	0.06318	0.063428	0.063553	0.063631	0.06372	0.063808	0.063824	0.063919	0.063952	0.064003
indentazione12	0.063644	0.063823	0.063942	0.064012	0.064061	0.06416	0.064175	0.064278	0.064237	0.064273

Indentation modulus

Eit/MPa	Ciclo 1	Ciclo2	Ciclo3	Ciclo4	Ciclo5	Ciclo6	Ciclo7	Ciclo8	Ciclo9	Ciclo10
indentazione1	50534.07	51664.56	52083.92	51740.56	51496.15	52116.03	53482.58	53401.13	51903.89	52380.15
indentazione2	55681.17	56010.57	55047.17	57048.64	55416.12	56031.26	56823.32	56302.68	53741.33	53119.29
indentazione3	54515.64	53912.94	53400.8	53646.04	54968.63	54302.42	53530.98	53921.52	52829.5	54738.65
indentazione4	53330.43	52367.83	53675.99	53760.78	53309.05	53520.05	52973.37	53952.29	53177.2	54663.34
indentazione5	50724.37	48660.16	49513.52	50235.78	49468.95	49984.39	50436.9	50732.02	51269.54	51045.1
indentazione6	53584.17	53409.11	54065.7	53741.95	53423.77	53233.07	54690.39	53687.9	54200.04	53297.16
indentazione7	54564.24	53748.66	54601.49	53270.55	52860.19	54068.81	54862.64	54395.48	53593.03	53781.62
indentazione8	54887.42	55402.72	55423.64	54895.18	55530.38	56215.15	55408.89	55649.12	55737.05	56883.47
indentazione9	48736.01	49343.79	49444.66	49275.93	49006.66	49378.48	50234.76	50208.73	49586.44	50227.3
indentazione10	67698.84	69027.33	67103.03	66991.97	67275.81	67896.42	67396.04	67614.13	68735.74	68282.09
indentazione11	49058.75	49852.91	49621.32	49444.62	49622.73	50030.93	49437.75	49864.81	49880.69	49992.58
indentazione12	64948.54	64359.41	64484.13	64359.21	64016.39	64589.33	64166.53	65260.44	63694.34	63888.99

Indentation hardness

Hit/MPa	Ciclo 1	Ciclo2	Ciclo3	Ciclo4	Ciclo5	Ciclo6	Ciclo7	Ciclo8	Ciclo9	Ciclo10
indentazione1	867.5007	867.3086	860.9934	860.8471	860.9625	859.2614	856.0486	855.9452	856.9879	855.8234
indentazione2	747.3709	743.8776	740.8701	736.3605	737.4823	734.2226	731.9488	731.0631	732.2422	730.5856
indentazione3	740.337	735.8509	733.6183	731.4173	728.6396	728.0591	728.2031	727.3421	727.4891	724.8609
indentazione4	746.8132	746.0185	742.1757	740.537	739.7505	738.5069	738.3245	737.7765	736.6905	734.69
indentazione5	845.9484	843.9548	841.3373	838.7472	839.592	838.6422	837.2756	836.2984	835.2269	835.5351
indentazione6	855.5042	850.9917	847.7414	846.3572	845.3266	844.6469	841.5826	842.4987	841.1048	841.9758
indentazione7	871.7503	867.9496	864.085	864.0064	863.394	861.3898	858.5203	858.5591	859.0663	857.9887
indentazione8	854.1003	848.7635	845.9412	844.2118	841.7319	839.7793	839.7411	839.2633	837.8151	835.5683
indentazione9	1028.925	1021.53	1017.699	1015.953	1015.254	1012.303	1008.017	1007.624	1008.045	1005.942
indentazione10	998.7655	994.2552	995.041	993.3754	992.8427	992.0544	991.0064	988.3303	986.8895	986.3739
indentazione11	1021.374	1013.433	1009.427	1006.976	1007.526	1001.381	1000.884	997.9074	996.8864	995.2802
indentazione12	1006.552	1000.909	997.2005	995.0245	993.4993	991.2678	989.9729	986.7898	988.0638	987.7875